Mechanisms of Tempered Martensite Embrittlement in Low Alloy Steels

R. M. HORN AND ROBERT O. RITCHIE

An investigation into the mechanisms of tempered martensite embrittlement (TME), also know as "500°F" or "350°C" or one-step temper embrittlement, has been made in commercial, ultra-high strength 4340 and Si-modified 4340 (300-M) alloy steels, with particular focus given to the role of interlath films of retained austenite. Studies were performed on the variation of i) strength and toughness, and ii) the morphology, volume fraction and thermal and mechanical stability of retained austenite, as a function of tempering temperature, following oil-quenching, isothermal holding, and continuous air cooling from the austenitizing temperature. TME was observed as a decrease in both K_{Ic} and Charpy V-notch impact energy after tempering around 300°C in 4340 and 425°C in 300-M, where the mechanisms of fracture were either interlath cleavage or largely transgranular cleavage. The embrittlement was found to be concurrent with the interlath precipitation of cementite during tempering *and* the consequent mechanical instability of interlath films of retained austenite during subsequent loading. The role of silicon in 300-M was seen to retard these processes and hence retard TME to higher tempering temperatures than for 4340. The magnitude of the embrittlement was found to be significantly greater in microstructures containing increasing volume fractions of retained austenite. Specifically, in 300-M the decrease in K_{Ic}, due to TME, was a 5 MPa$\sqrt{m}$ in oil quenched structures with less than 4 pct austenite, compared to a massive decrease of 70 MPa$\sqrt{m}$ in slowly (air) cooled structures containing 25 pct austenite. A complete mechanism of tempered martensite embrittlement is proposed involving i) precipitation of interlath cementite due to partial thermal decomposition of interlath films of retained austenite, and ii) subsequent deformation-induced transformation on loading of remaining interlath austenite, destabilized by carbon depletion from carbide precipitation. The deterioration in toughness, associated with TME, is therefore ascribed to the embrittling effect of i) interlath cementite precipitates and ii) an interlath layer of mechanically-transformed austenite, *i.e.*, untempered martensite. The presence of residual impurity elements in prior austenite grain boundaries, having segregated there during austenitization, may accentuate this process by providing an alternative weak path for fracture. The relative importance of these effects is discussed.

IT has been well known for many years that high strength martensitic steels, heat-treated to achieve optimum combinations of strength, ductility, and toughness, are susceptible to embrittlement during tempering.[1-4] This loss in toughness can result primarily from two types of thermal treatments: i) holding or slow cooling alloy steels, previously tempered above 600°C, in the temperature range 350 to 550°C (temper embrittlement), and ii) tempering as-quenched alloy steels in the range 250 to 450°C (tempered martensite embrittlement). Whereas there is now a large body of evidence linking the phenomenon of temper embrittlement to the grain boundary weakening effect of segregated impurities or "tramp" elements (*e.g.*, S, P, Sb, Sn, and so forth[1,2,4]), the mechanism of tempered martensite embrittlement (TME), also known as "500°F" or "350°C" or "one-step temper embrittlement" has remained somewhat of a mystery. The embrittlement has traditionally been seen as a sudden decrease in ambient temperature Charpy V-notch impact energy and an increase in the Charpy transition temperature during tempering, and was historically associated with an increase in intergranular fracture during failure.[5-8] Fracture toughness and tensile ductility were also seen to be degraded in certain steels, but such measurements were not always consistent in revealing the embrittlement.[3,9,10]

Early explanations of TME were linked to the transformation during tempering of austenite, retained after quenching.[11] However, this was largely discounted since it was realized that i) refrigeration of the steel after quenching (which was presumed to remove most of the retained austenite) did not eliminate the phenomenon,[7,12] and ii) transformation of retained austenite could not readily account for the incidence of intergranular fracture which was observed.[5] However, later work on higher alloy steels revealed that fractures in the embrittlement range were not always intergranular; mechanisms such as cleavage,[13,15] quasicleavage,[9,17] fibrous,[16] mixed ductile-brittle,[14,48] martensite "translath",[14] and martensite "interlath/packet"[18] failures have been reported. Grossmann[5] was probably the first author to suggest a more definite link between the sequence of carbide precipitation and TME. This was substantiated by Klinger and coworkers[8] who found

R. M. HORN is Associate Development Engineer, Department of Materials Science and Mineral Engineering, University of California, Berkeley, CA 94720. ROBERT O. RITCHIE is Associate Professor, Department of Mechanical Engineering, Massachusetts Institute of Technology, Cambridge, MA 02139. Both authors were formerly with the Lawrence Berkeley Laboratory, University of California.

Manuscript submitted December 19, 1977.

ISSN 0360-2133/78/0810-1039$00.75/0
© 1978 AMERICAN SOCIETY FOR METALS AND THE METALLURGICAL SOCIETY OF AIME

that embrittlement was concurrent with the formation of platelet cementite, replacing ϵ-carbide, and that TME was time-dependent at differing tempering temperatures, *i.e.*, tempering at longer times somewhat below the characteristic embrittling temperature also resulted in embrittlement. This time-dependence of TME was further verified by studies which showed that rapid induction heating and cooling would suppress the embrittlement.[19] Several other workers related the onset of TME to the formation of coarsening of cementite films, which were generally observed to form at grain and lath boundaries.[19-22] This important role of carbide precipitation on TME was supported by work on high-strength steels modified with silicon and aluminum.[13,23-26] Both these elements are known to retard the replacement of ϵ-carbide by cementite to higher tempering temperatures.[26,27] It was found that in such modified steels the embrittlement trough was correspondingly displaced to higher temperatures. Other authors suggested that a high dislocation density, in addition to coarse carbide precipitation, was essential for embrittlement.[9,28,29] King *et al.*[17] furnished evidence for this interaction by finding that the TME trough was increased to higher tempering temperatures in steels fractured below room temperature.

Because of the incidence of intergranular fracture in many TME failures, other theories of the phenomenon have focussed on the role of grain boundary segregation of residual impurity elements.[3,30-32] For example, it was found that alloying additions of chromium and manganese and the presence of certain impurity elements, phosphorus and nitrogen, increased the level of embrittlement.[30] Subsequently, the presence of segregated P and N on TME intergranular fracture surfaces was directly identified using Auger spectroscopy.[32] However, the role of impurities on TME was demonstrated most convincingly when tests were conducted on laboratory-made high purity steels of the same nominal composition as susceptible commercial steels, and the embrittlement phenomenon was not observed at room temperature*. This prompted Banerji *et al.*[32] to propose that the mechanism of TME was essentially similar to that of temper embrittlement, involving the segregation* of residual impurities, in this instance P and N, to prior austenite grain boundaries promoted by the co-segregation of Mn and possibly Si. Furthermore, attempts were made to rationalize a combined role of impurities and carbide precipitation by suggesting that during the growth of carbides, impurity elements are rejected giving rise to a local increase in impurity concentration at carbide/matrix interfaces. More recently, attention has once more focused on the role of retained austenite on TME based on new data concerning the distribution, morphology, and thermal and mechanical stability of retained austenite during tempering.[13,18,33] The objective of the present investigation is to reassess this role of retained austenite in the light of this new information, and to attempt to elucidate specific mechanisms of TME* in commonly-utilized commercial ultra-high strength steels. While we acknowledge that the embrittlement of a given steel cannot be attributed to a single mechanism, such as interlath carbide precipitation, decomposition of retained austenite, or impurity segregation, and is almost certainly due to a combination of several factors, our aim is to clearly demonstrate the role of retained austenite as a major contributing feature in promoting the onset of tempered martensite embrittlement.

* Later work showed that the TME embrittlement trough reappears for tests at −196°C.[47]

*Such segregation has recently been shown to occur during prior austenitization,[32,47] rather than during tempering, as is generally the case for temper embrittlement.

*This term will be applied to the embrittlement phenomena observed realizing it is not unique to *fully* martensitic steels.

EXPERIMENTAL PROCEDURES

The materials investigated were two commercial ultra-high strength steels, AISI 4340 and 300-M, of composition in weight percentages shown below:

	C	Mn	Cr	Ni	Mo	Si	S	P	V	Cu
4340	0.41	0.80	0.79	1.75	0.23	0.26	0.004	0.006	–	0.06
300-M	0.42	0.76	0.76	1.76	0.41	1.59	0.002	0.007	0.10	–

The composition of 300-M is essentially that of 4340, modified with 1.3 wt pct silicon. Both heats were of aircraft quality (vacuum-arc remelted) and were received as hot-rolled bar in the fully annealed condition. Before heat-treatment, as-received material was hot forged and hot rolled to desired thicknesses and subsequently slow-cooled and spheroidized at 650°C to achieve good machinability. Test specimens were austenitized at 870°C for 1 h and then given one of three cooling treatments (Fig. 1), namely i) direct quenched in agitated oil, ii) slow continuously cooled at a rate equivalent to that experienced by 1 in. (25 mm) or 2 in. (50 mm) plate during air-cooling, or iii) isothermally transformed by holding at 250°C* for 1 h before oil quenching (equivalent to martempering).

*Isothermal holding temperature (250°C) represents a transformation temperature of 50°C below M_S for 4340 and 20°C below M_S for 300-M.

Table I lists the cooling treatments of interest for the respective steels. Test specimens were subsequently tempered for 1 h in the temperature range 200

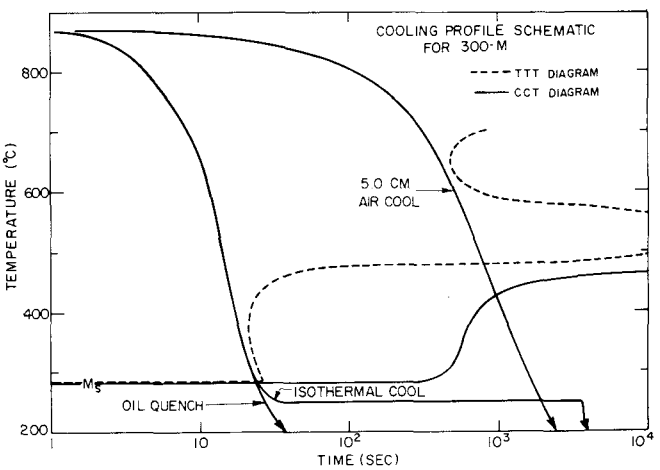

Fig. 1—Schematic diagram displaying cooling treatments investigated on transformation diagram for 300-M steel.

to 650°C. The prior austenite grain size of all structures was approximately 20 μm. Ambient temperature uniaxial tensile properties were determined using 25.4 mm gage length cylindrical and flat tensile bars, and plane strain fracture toughness (K_{Ic}) values were determined using 25.4 mm thick 1-T compact tension specimens, in accordance with appropriate ASTM standards. K_{Ic} measurements were found to be valid, with respect to such standards, for all tests except for

Table I. Heat-Treatments Investigated

Steel	Cooling Treatment After Austenitization for 1 h at 870°C	Designation
300-M	Oil quenched	300-M-QT
300-M	Isothermally held for 1 h at 250°C	300-M-ISO
300-M	Slow continuously cooled to simulate air-cooling of 50 mm thick plate	300-M-AC
4340	Oil quenched	4340-QT
4340	Slow continuously cooled to simulate air cooling of 25 mm thick plate	4340-AC

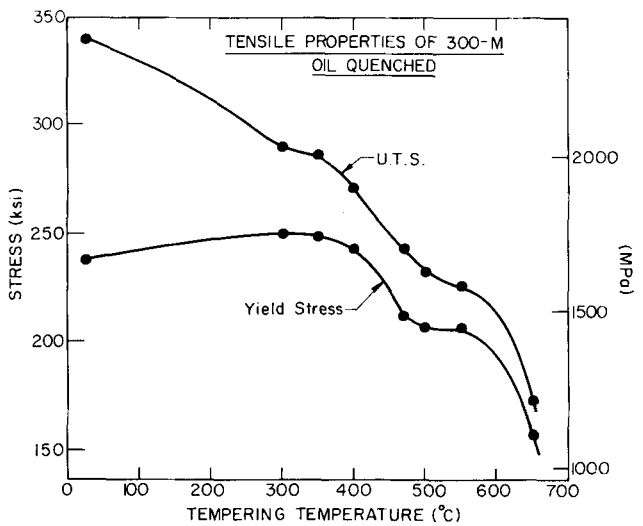

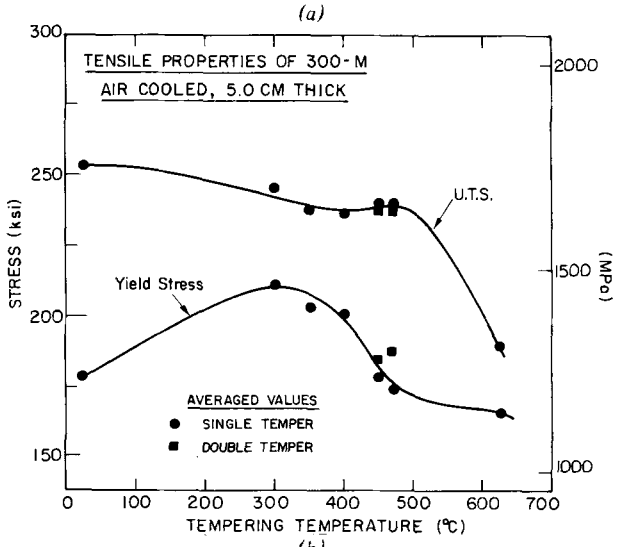

Fig. 2—Effect of tempering temperature on the room temperature uniaxial tensile properties for heat treatments investigated (*a*) oil quenched 300-M steel, (*b*) air-cooled, (50 mm thick section), 300-M steel, (*c*) isothermally-held (at 250°C, 1 h), 300-M steel, (*d*) oil-quenched 4340 steel, and (*e*) air-cooled (25 mm thick section), 4340 steel. (All steels austenitized for 1 h at 870°C prior to cooling.)

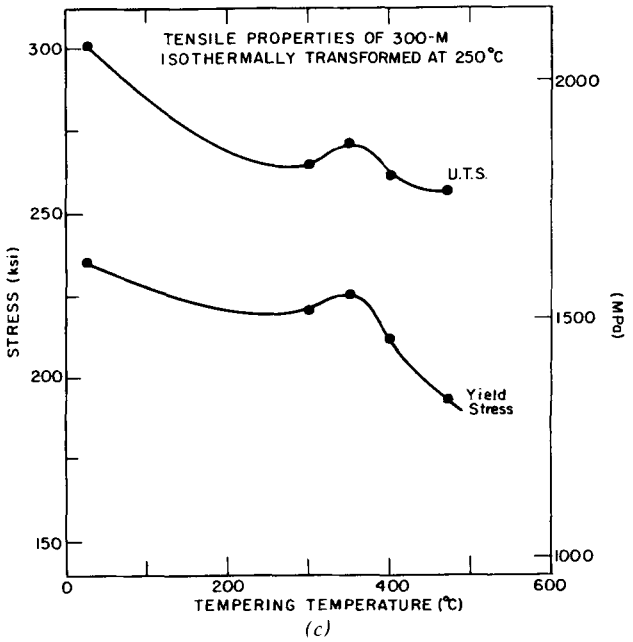

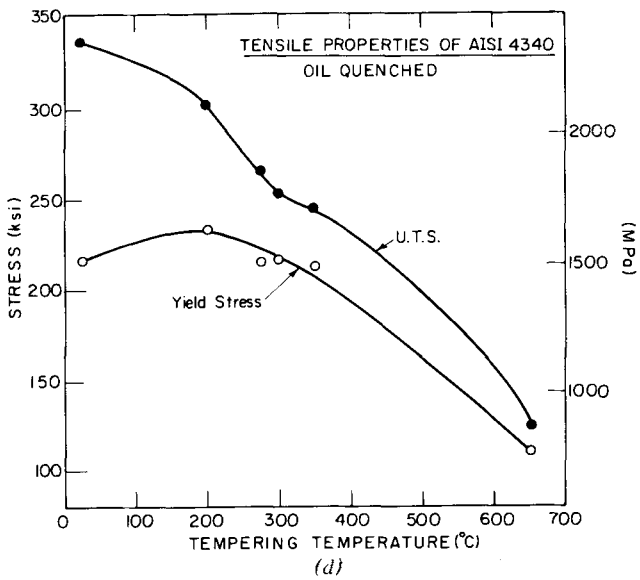

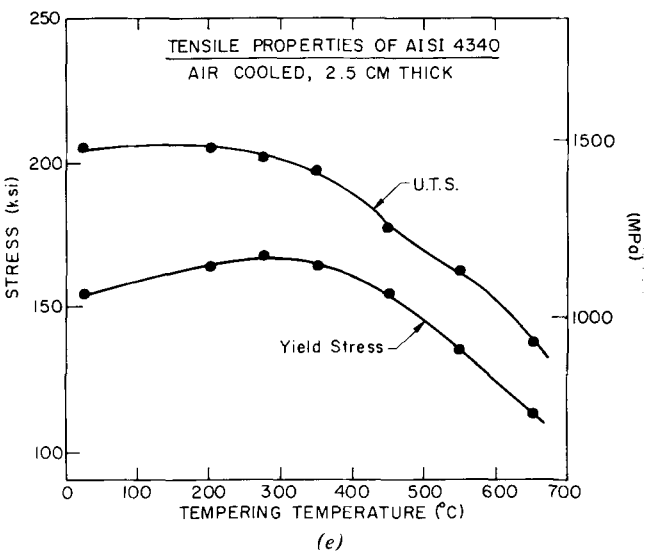

specimens tempered at 650°C. The toughness of the latter structures was estimated using i) equivalent energy procedures at maximum load,[34] and ii) measurement of J_{Ic} values,[35] at initiation of fracture, detected using the electrical potential method.[36] ASTM standard Charpy V-notch impact tests were also conducted to compare with fracture toughness results. All test specimens were machined in the longitudinal L-T orientation from rolled bar.

Microstructures were characterized using optical and transmission electron microscopy, and fracture surface morphology was assessed using scanning electron microscopy. Levels of retained austenite in the structures investigated were measured using standard X-ray techniques[37] and magnetic saturation induction measurements.[38] Volume fractions of austenite determined by these two methods agreed to within ±1 pct. The mechanical stability of austenite, with respect to deformation, was assessed by continuously monitoring the magnetic saturation of the steel during uniaxial tensile tests. Calibration methods using austenite-free standards were utilized to determine initial austenite levels. The distribution and morphology of the retained austenite was characterized by standard bright and dark field imaging with transmission electron microscopy. Carbide type was identified from from analysis[39] of diffraction patterns of extraction replicas taken from polished and over-etched metallographic specimens.

RESULTS

The heat treatments investigated, namely oil quenching, air cooling, and isothermal holding after austenitization, are illustrated schematically in Fig. 1, and are listed in Table I. Uniaxial tensile properties at ambient temperature for the five treatments are shown in Fig. 2 as a function of tempering temperature. Oil quenched 300-M (300-M-QT) develops peak strength after tempering at 300°C (Fig. 2(a)), and is significantly stronger than the air-cooled (300-M-AC) and isothermally-held (300-M-ISO) structures. Peak strength for the latter treatments is also attained after tempering at 300°C (Fig. 2(b) and (c)). AISI 4340, of lower silicon content than 300-M, develops a peak strength condition after tempering at 200°C (Fig. 2(d) and (e)) with the oil quenched structures (4340-QT) being significantly stronger than air-cooled structures (4340-AC). It is apparent that the increased silicon content in 300-M leads to i) higher overall strength levels than in 4340, due to solid solution strengthening and ii) a change in the kinetics of tempering[27] which shifts the optimum tempering temperature for peak strength from 200°C in 4340 to 300°C in 300-M*. Although tensile properties vary consistently with tempering temperature for all treatments, the nature of the cooling treatment has a significant influence on microstructure and fracture properties. These effects are summarized for the individual treatments.

*These tempering temperatures correspond to the commercially-used treatments after oil quenching.

A) 300-M Steel–Oil Quenching Treatment (300-M-QT)

The variation of plane strain fracture toughness (K_{Ic}) with tempering temperature for oil-quenched 300-M (300-M-QT) is shown in Fig. 3. Although in the as-quenched (untempered) condition, the toughness is low (K_{Ic} = 35 MPa$\sqrt{m}$), the fracture toughness in-

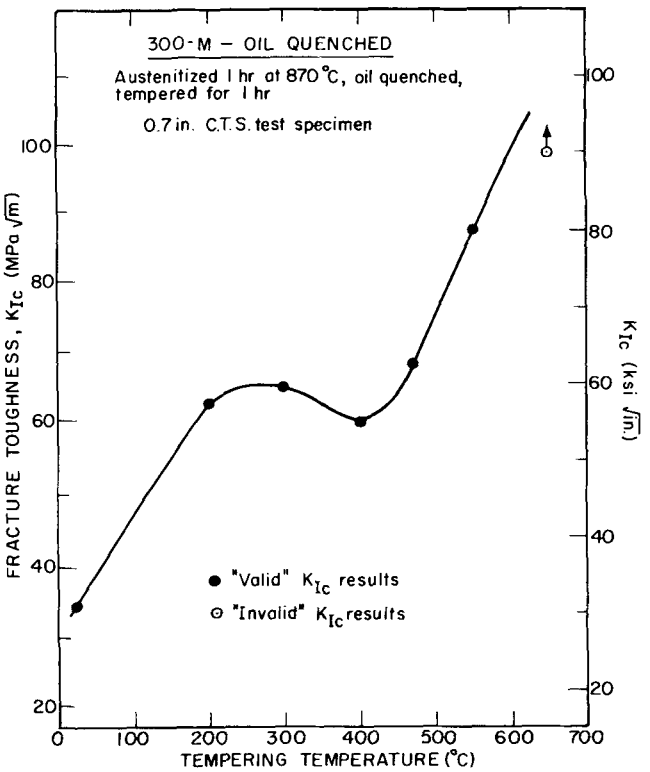

Fig. 3–Effect of tempering temperature on the room temperature plane strain fracture toughness (K_{Ic}) of 300-M steel, oil quenched.

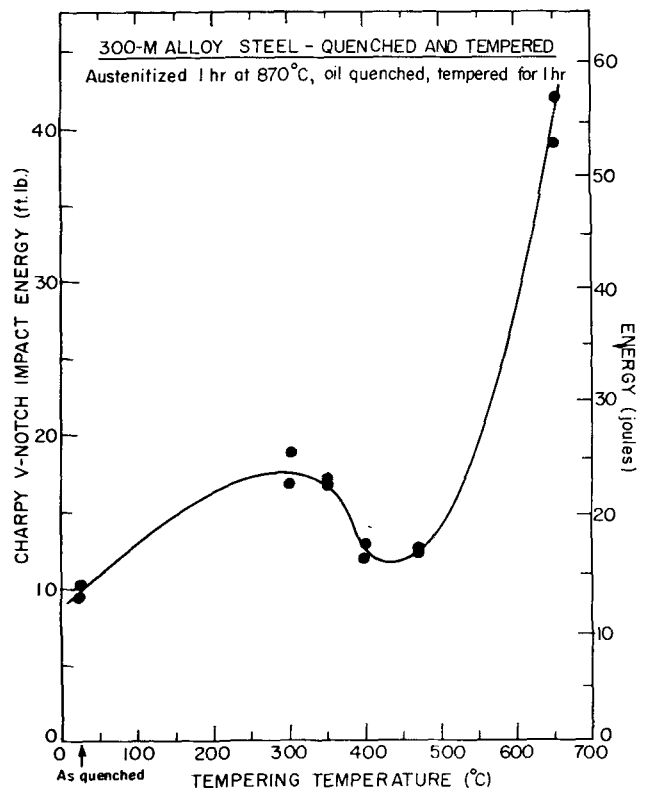

Fig. 4–Effect of tempering temperature on the room temperature Charpy V-notch impact energy of 300-M steel, oil quenched.

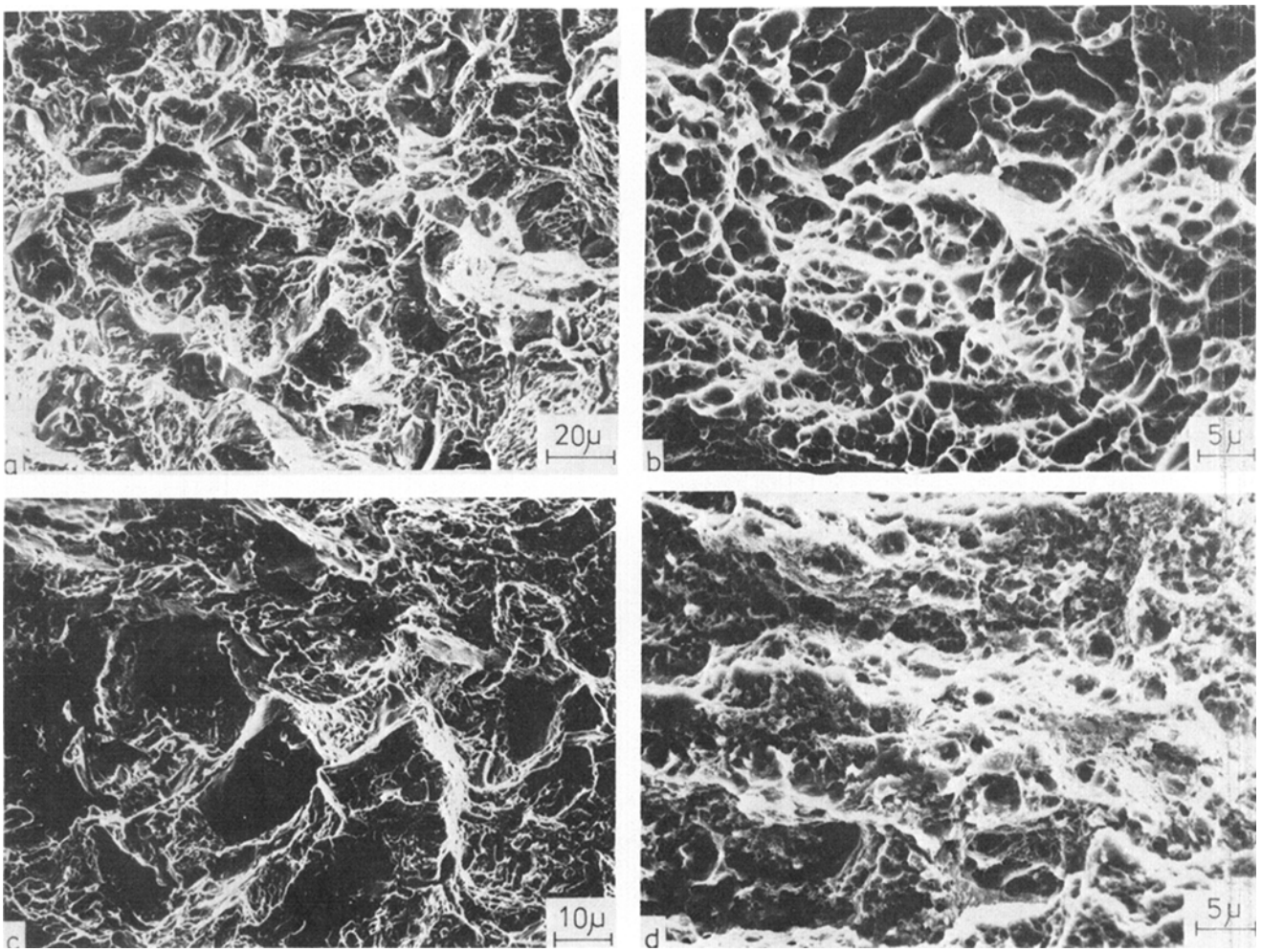

Fig. 5–Mechanisms of failure in 300-M steel, oil-quenched in (*a*) untempered condition showing a mixture of ductile rupture, quasicleavage, and intergranular fracture, (*b*) tempered at 300°C displaying ductile rupture, (*c*) tempered at 400°C showing transgranular cleavage with ductile rupture, and (*d*) tempered at 650°C, displaying ductile rupture.

creases rapidly to 65 MPa$\sqrt{m}$ after tempering at 300°C. Tempering at a higher temperature of 400°C results in a slight degradation in K_{Ic}, despite the fact that the strength is also decreasing (Fig. 2(*a*)). This "toughness trough," also observed in Charpy V-notch impact energy data (Fig. 4), is an example of tempered martensite embrittlement (TME). Note, however, that the embrittlement in the quenched and tempered steel results in only a small drop in toughness (~5 MPa$\sqrt{m}$). Tempering at temperatures above 400°C leads to a significant increase in toughness as the strength of the steel drops. The variation of fracture mode with tempering temperature is shown in Fig. 5. As-quenched structures failed by a mixture of ductile rupture (microvoid coalescence), intergranular and transgranular cleavage (Fig. 5(*a*)). Structures tempered at 300°C (the 'top' of the TME trough), and at 400°C (the 'bottom' of the TME trough) failed by ductile rupture (Fig. 5(*b*) and (*c*)), with some evidence of transgranular cleavage at 400°C. Failure in structures tempered at 650°C was by 100 pct ductile rupture (Fig. 5(*d*)).

The microstructure of oil-quenched 300-M, shown in Fig. 6 for the as-quenched condition, was a martensitic lath structure, with some twinning, and contained evidence of almost continuous thin films (100 to 200Å thick) of retained austenite surrounding the laths. The hardening carbide was identified as ϵ-carbide at the 300°C condition, and cementite at tempering conditions above 400°C. The stability of the retained austenite was found to be a strong function of thermal history and loading conditions (Fig. 7). Shown in this figure is the variation with tempering temperature of the volume fraction of retained austenite, measured using magnetic saturation techniques,* i) in the unstressed microstructure, ii) after 0.2 pct (strain (*i.e.*, at yield), and iii) after 2 pct strain. It is important at this stage to distinguish between the variation of the percentage of austenite in unstressed (prior to loading) structures, which represents the *"thermal stability"* of retained austenite with respect to tempering temperature, and the variation of austenite percentage after strain, which represents the *"mechanical stability"* of retained austenite* with respect to tempering temperature. Considering first thermal stability, it is apparent that approximately 6 pct is retained after oil quenching, 4 pct of which remain stable with tempering up to temperatures of 400°C. Above 470°C, decomposition of austenite during tempering is essentially com-

*Initial volume fractions of austenite were verified using X-ray techniques.[37]

*Mechanical stability as used refers to austenite stability to post-transformation deformation as opposed to stabilization by transformation stresses.

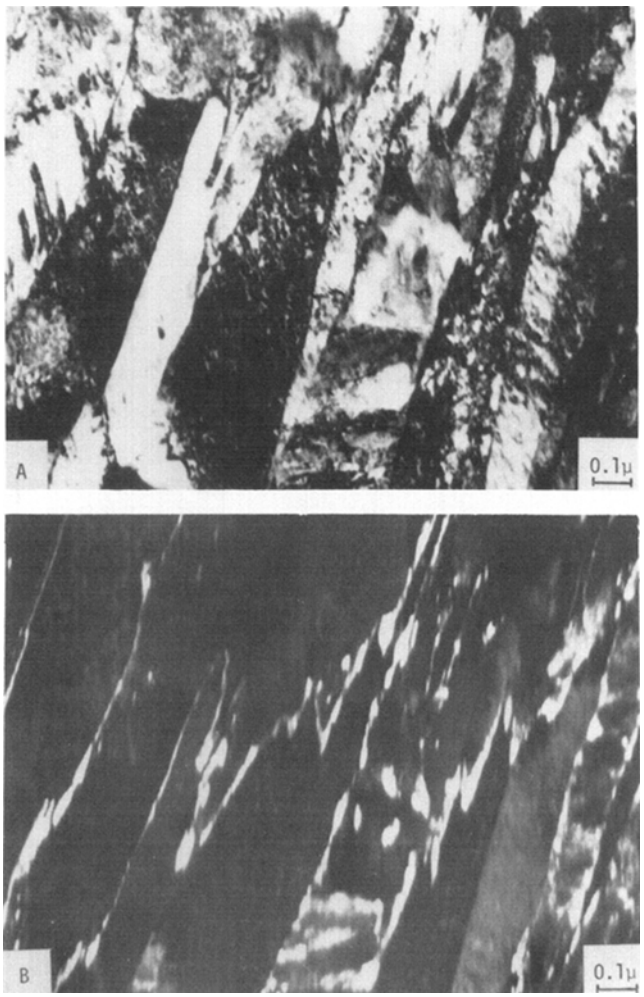

Fig. 6—Transmission electron microscopy of 300-M, direct oil-quenched from 870°C showing retained austenite films surrounding martensite laths: (*a*) bright field image and; (*b*) dark field image of austenite reflection, showing contrast reversal.

plete. The mechanical stability of the austenite, seen by comparing unstressed levels with those after 0.2 and 2.0 pct strain, is somewhat different. It is clear that austenite present in the untempered structure is extremely unstable, since all but 1 pct of the original retained austenite has transformed by yield (0.2 pct strain). Mechanical stability is largest for tempering temperatures around 300 to 350°C, but the retained austenite becomes mechanically destabilized again at 400°C, which corresponds to the tempering temperature where TME occurs.

B) 300-M Steel–Air Cooling (300-M-AC) and Isothermal (300-M-ISO) Treatments

The variations in fracture toughness with tempering temperature for the 300-M-AC and 300-M-ISO treatments are shown in Figs. 8 and 9, indicating similar trends to that exhibited for the oil-quenched treatment (300-M-QT) as shown in Fig. 3. The peak toughness values are again achieved after tempering at 300°C, but are significantly higher ($K_{Ic} \sim 90$ MPa$\sqrt{m}$) consistent with the fact that the air-cooled and isothermally-transformed structures are of lower strength. However, the most significant difference is that the tempered martensite embrittlement trough, which occurs now at around 470°C, is strikingly larger, *i.e.*, a toughness drop of between 35 to 45 MPa$\sqrt{m}$ for these conditions compared with the 5 MPa$\sqrt{m}$ toughness drop in the oil-quenched structures (Fig. 3). Charpy V-notch energy curves revealed identical trends.[13] Fracture mechanisms were similar for the 300-M-AC and 300-M-ISO treatments. Structures tempered at 300°C (the 'top' of the TME trough) failed by ductile rupture, whereas at 470°C (the 'bottom' of the TME trough) failure occurred by a lath boundary cleavage separation mechanism (Fig. 10). Note the absence of intergranular fracture associated with TME, as was the case for oil-quenched structures.

The microstructures of the 300-M-AC and 300-M-ISO structures were also very similar, but significantly different from oil-quenched material. Shown in Fig. 11 are bright and dark field electron micrographs of the 300-M-AC condition, after tempering at 300°C, which indicate a primarily bainitic structure containing a large fraction of thick (~500Å) interlath films of retained austenite. The principal hardening carbide for both treatments was identified as ϵ-carbide after tempering at 300°C, and cementite at 470°C. The thermal and mechanical stability of the austenite with respect to tempering temperature is shown in Figs. 12 and 13 for the 300-M-AC and 300-M-ISO treatments, respectively. It is clear that the volume fraction of retained austenite (before deformation) in these structures is significantly greater than in oil quenched structures (see Fig. 7), 13 to 16 pct remaining stable up to tempering temperatures of 425°C. Above this temperature, initial austenite levels decrease quite rapidly as decomposition occurs during tempering at the higher temperatures. The mechanical stability of the aus-

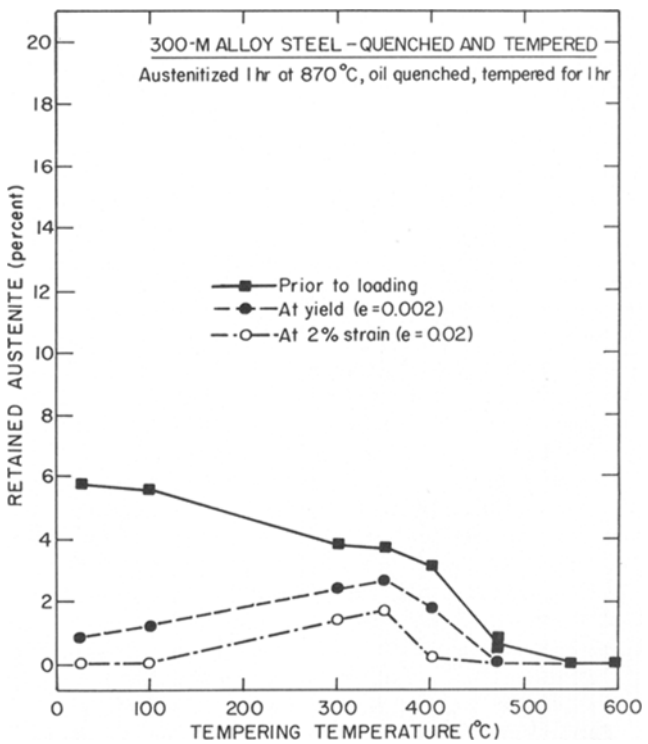

Fig. 7—Variation of percentage of retained austenite, measured by magnetic saturation, with tempering temperatures for oil-quenched, 300-M steel. Plotted are initial (unstressed) level and amounts untransformed at 0.2 pct strain (*i.e.*, at yield) and at 2.0 pct strain.

tenite with respect to tempering temperature is similar for both 300-M-AC and 300-M-ISO treatments, and follows the same trend shown by oil-quenched structures (Fig. 7). In the untempered state, retained austenite is again unstable mechanically (all 15 pct is transformed by 2 pct strain in the 300-M-ISO condition), whereas after tempering at 300°C it becomes very stable. Marked mechanical destabilization can be seen to occur at tempering temperatures above 425°C; temperatures which are associated with the onset of tempered martensite embrittlement (Figs. 8 and 9). Thus, it is apparent for 300-M steel that the severity of TME is directly related to the volume fraction of retained austenite, and that onset of the embrittlement coincides with the tempering temperature at which austenite becomes mechanically unstable with respect to deformation.

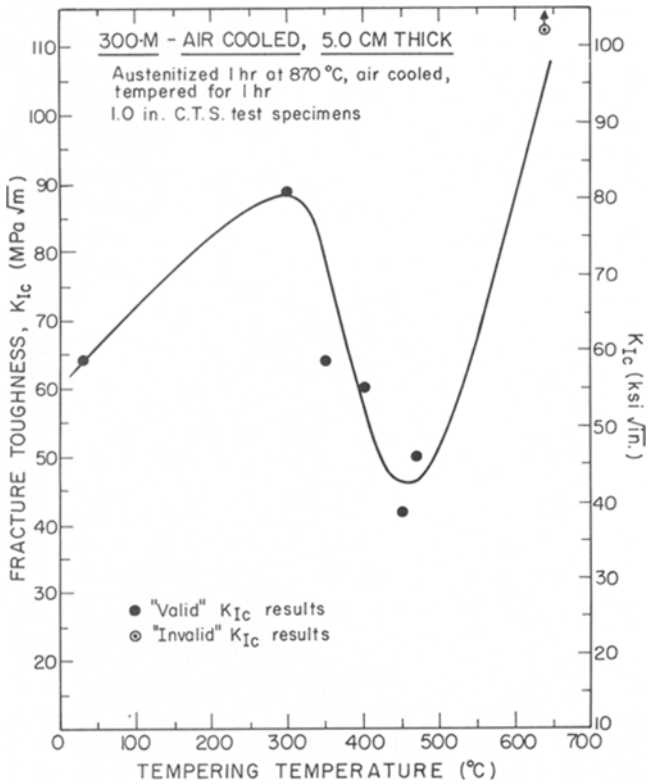

Fig. 8—Effect of tempering temperature on the room temperature plane strain fracture toughness of 300-M steel, air-cooled (50 mm thick plate).

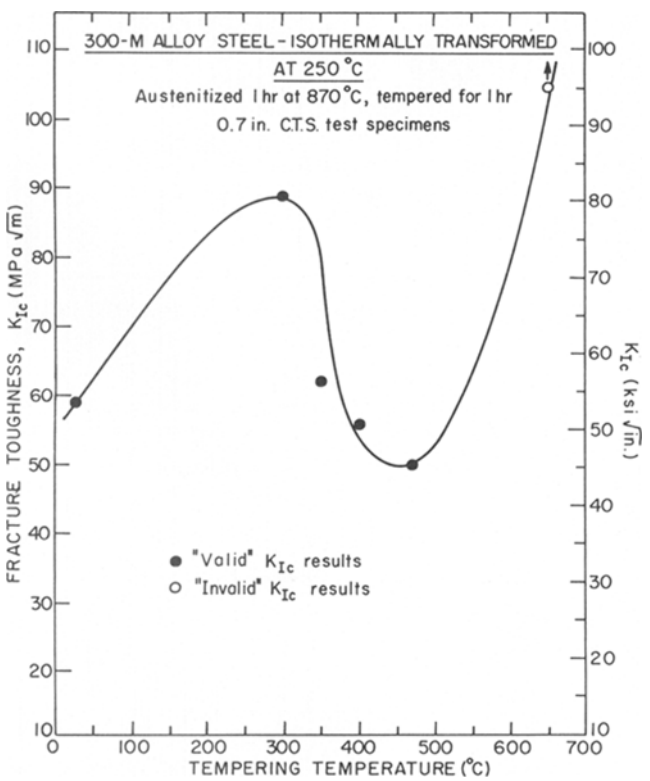

Fig. 9—Effect of tempering temperature on the room temperature plane strain fracture toughness of 300-M steel, isothermally held at 250°C, 1 h.

C) AISI 4340 Steel—Oil-Quenched (4340-QT) and Air-Cooling (4340-AC) Treatments

As a consequence of lower silicon content, the characteristics of heat-treated 4340 steel are somewhat different from 300-M. In addition to exhibiting lower strength levels, the variation of toughness in 4340 with tempering temperature, shown in Fig. 14 for the oil-quenched (4340-QT) condition and in Fig. 15 for the air-cooled (4340-AC) condition, has the same general trend as that shown by 300-M. The temperature dependence of the behavior, however, has shifted. This is a consequence of the role of silicon[27] in 300-M, which

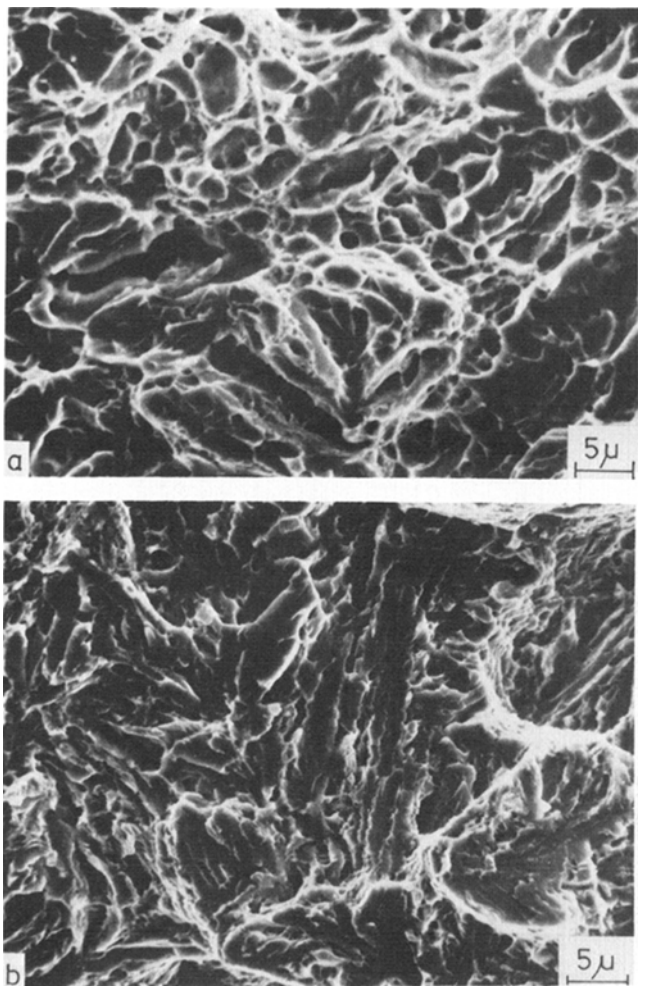

Fig. 10—Mechanisms of failure in 300-M, isothermally-held and (*a*) tempered at 300°C showing ductile rupture and (*b*) tempered at 470°C displaying interlath cleavage.

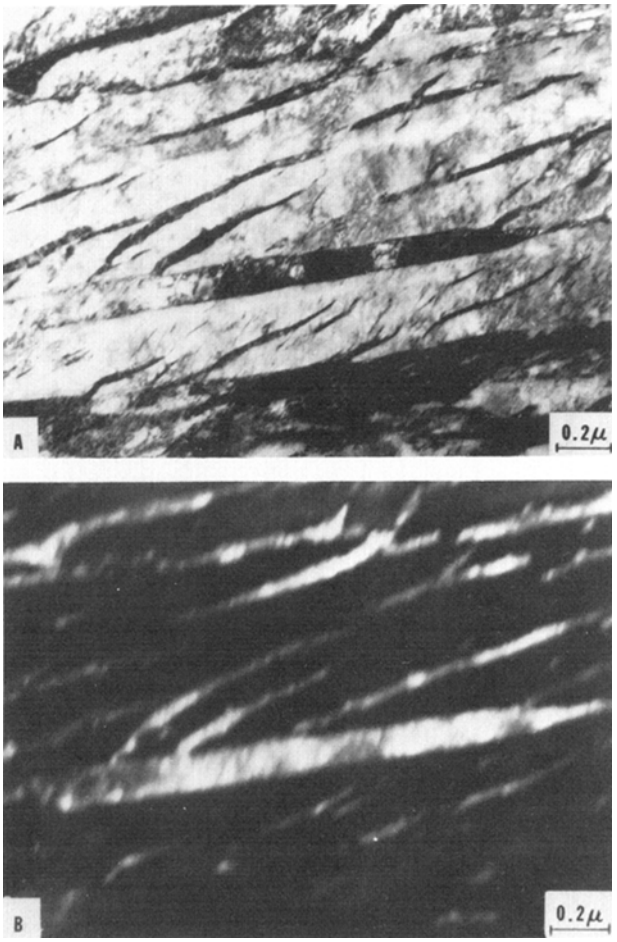

Fig. 11—Transmission electron microscopy of 300-M, air-cooled and tempered at 300°C, showing retained austenite films on bainitic-martensitic matrix: (*a*) bright field image; and (*b*) dark field image of austenite reflection reversing contrast.

retards the formation of cementite and extends the temperature at which ϵ-carbide exists. Accordingly, peak strength and toughness in 4340 are achieved after tempering at 200°C instead of at 300°C in 300-M, and the TME trough, which can be seen to be particularly small, is similarly displaced to lower tempering temperatures around 275°C. Charpy V-notch energy measurements revealed identical trends.[13]

The fracture mechanisms of structures tempered at 200°C and 275°C (the 'top' and 'bottom' of the TME trough, respectively), are shown in Fig. 16 for the 4340-AC structure. At 200°C, failure occurs by ductile rupture with isolated cleavage facets (Fig. 16(*a*)), whereas at 275°C the embrittled structure fails by a fully transgranular cleavage mechanism (Fig. 16(*b*)); no evidence of intergranular cracking was again detected.

Analysis of the microstructres in 4340-QT showed that, as with 300-M steel, the hardening carbide at peak strength and toughness (*i.e.*, after 200°C temper) was ϵ-carbide, whereas in the TME trough (*i.e.*, after tempering at 275°C) cementite was detected. Thin interlath films of retained austenite were present within a lath martensitic structure.[49]

The thermal and mechanical stability of retained austenite with respect to tempering temperature is shown in Figs. 17 and 18 for the 4340-QT and 4340-AC treatments, respectively. Clearly overall levels of austenite are significantly less than in 300-M (maximum volume fraction of 6 pct), and slow cooling after austenitizing (*i.e.*, with the 4340-AC treatment) does not yield increased volume fractions as was the case for 300-M. The austenite is reasonably stable to thermal decomposition up to tempering temperatures of 200°C, whereupon its thermal and mechanical stability decreases rapidly. Despite the shift to lower tempering temperatures caused by the lower silicon content compared to 300-M, the small magnitude of the TME trough is consistent with the smaller overall levels of retained austenite, and the tempering temperature for the onset of TME again coincides with destabilization of the austenite.

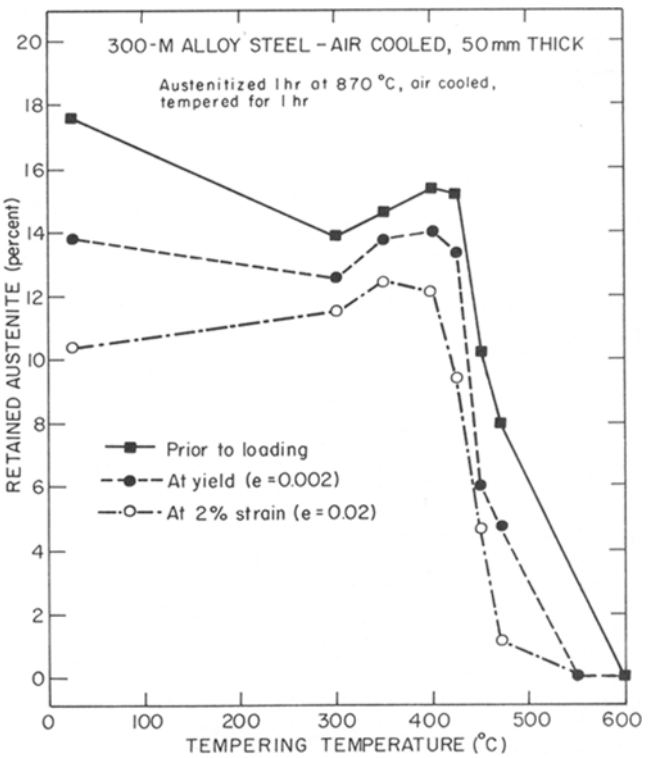

Fig. 12—Variation of percentage of retained austenite, measured by magnetic saturation, with tempering temperature for 300-M, air-cooled. (Unstressed, 0.2 pct strain, 2 pct strain levels shown.)

Table II. Summary of Tempered Martensite Embrittlement Phenomena

Steel and Treatment	Tempering Regime for Embrittlement	Maximum Toughness Drop, MPa$\sqrt{m}$	Tempering Regime for Austenite Destabilization	Austenite Level, Pct
300-M Oil quenched	~400°C	5	≥400°C	5
300-M Isothermally held at 250°C	~425°C	30	≥400°C	12
300-M 50 mm, air cooled	~450°C	40	≥425°C	14
300-M 100 mm, air cooled	~450°C	70	≥425°C	25
4340 Oil quenched	~275°C	5	≥250°C	5
4340 25 mm, air cooled	~275°C	5	≥275°C	4

DISCUSSION

As described in the Introduction to this paper, the currently held views on tempered martensite embrittlement are that the embrittlement is associated with the precipitation of cementite[5,8,18-22] and/or the segregation of residual impurity elements,[3,30-32] and that the original explanations based on the decomposition of retained austenite have been largely discounted[7,12,40]

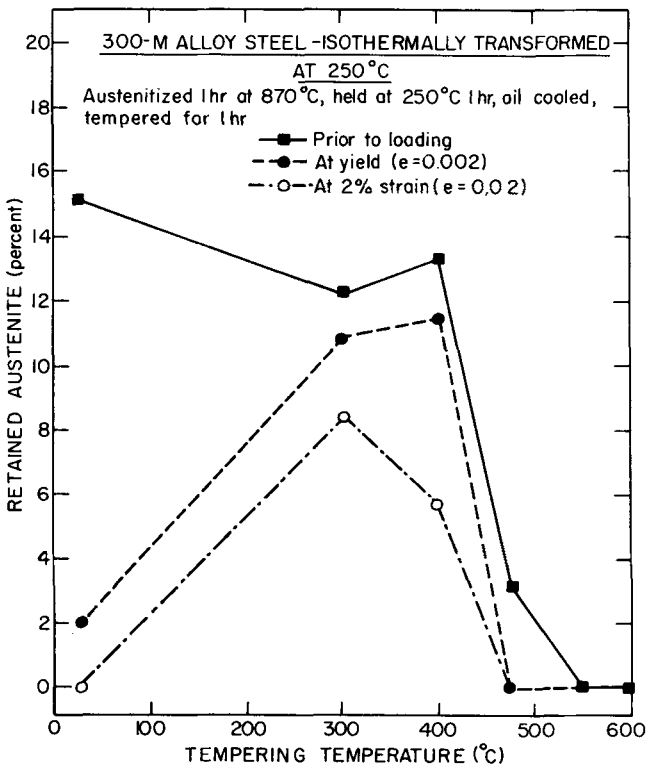

Fig. 13—Variation of percentage of retained austenite, with tempering temperature for 300-M, isothermally-held at 250°C, 1 h. (Unstressed, 0.2 pct strain, 2.0 pct strain levels shown.)

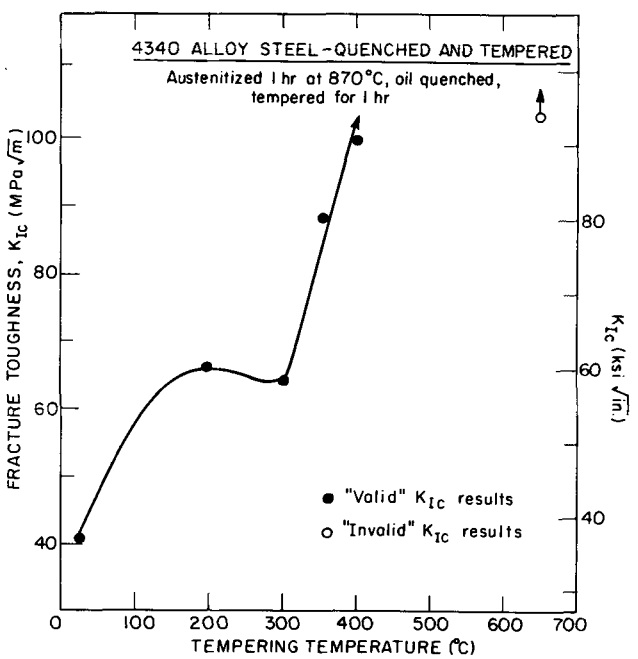

Fig. 14—Effect of tempering temperature on the room temperature plane strain fracture toughness of 4340 steel, oil quenched.

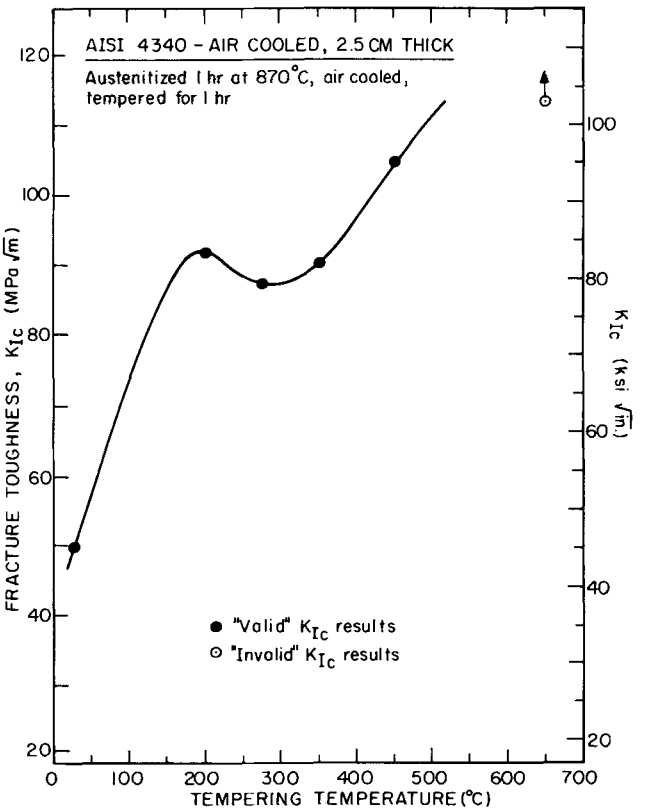

Fig. 15—Effect of tempering temperature on the room temperature plane strain fracture toughness of 4340 steel, air cooled (25 mm thick section).

or forgotten. However, it is quite clear from the present study that, depending on the thermal and mechanical stability of the austenite with respect to tempering temperature in 4340-type steels, the presence of retained austenite can play a major role in the onset and severity of the embrittlement (Table II). For each heat-treatment schedule investigated in both steels, the onset of TME coincides directly with the range of tempering temperature at which retained austenite becomes mechanically unstable with respect to deformation. Changing the silicon content of the steel, which changes the kinetics of carbide precipitation, has no effect on this correlation; the TME trough still occurs over the tempering temperature range where austenite becomes unstable. Furthermore, the magnitude of the embrittlement, in terms of the size of the decrease in K_{Ic}, is directly proportional to the amount of retained austenite present. Thus, air-cooled and isothermally-transformed structures, with their higher volume fractions of retained austenite, show significantly larger TME troughs than oil-quenched structures, *despite* the fact that such structures are of lower strength (Fig. 2). To test this further, specimens of 300-M were very slowly continuously cooled to simulate the air cooling of a 100 mm thick plate, where extremely high levels of austenite (~25 pct) are retained.[13] The resulting variation in K_{Ic} with tempering temperature (Fig. 19) indicates a massive TME trough, where K_{Ic} decreases from 110 MPa$\sqrt{m}$ at the 'top' of the trough (300°C temper) to a mere 40 MPa$\sqrt{m}$ at the 'bottom' (450°C temper). The onset of this 70 MPa$\sqrt{m}$ decrease in toughness once again was found to coincide with the tempering temperature range where retained austenite becomes mechanically unstable, and

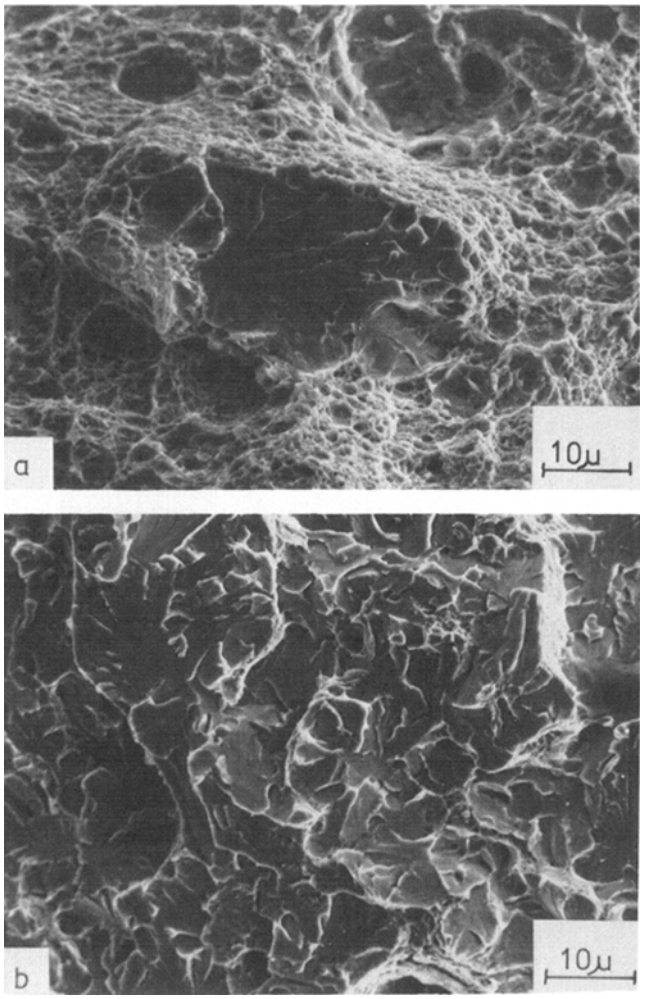

Fig. 16–Mechanism of failure in 4340, air cooled (*a*) tempered at 200°C displaying ductile rupture, and (*b*) tempered at 275°C displaying transgranular cleavage.

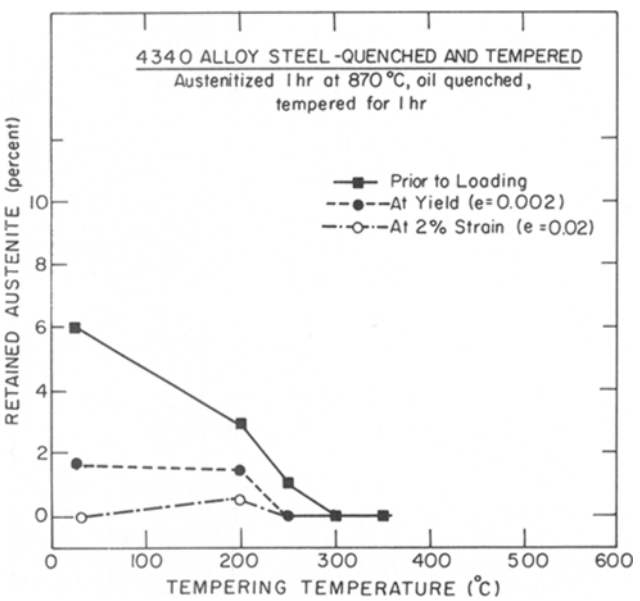

Fig. 17–Variation of percentage of retained austenite with tempering temperature for oil-quenched 4340 steel (unstressed, 0.2 pct strain, 2.0 pct strain levels shown).

again no evidence of intergranular failure would be detected in embrittled samples.[13] Clearly, mechanically destabilized retained austenite cannot be dismissed as one of the root causes of TME, and for 4340-type steels, the explanation based on retained austenite must be reevaluated.

Early investigations[7,12] discounted the role of retained austenite on TME because i) refrigeration treatments after austenitizing did not remove the embrittlement, and ii) the intergranular character of embrittled fracture surfaces seen in low alloy carbon

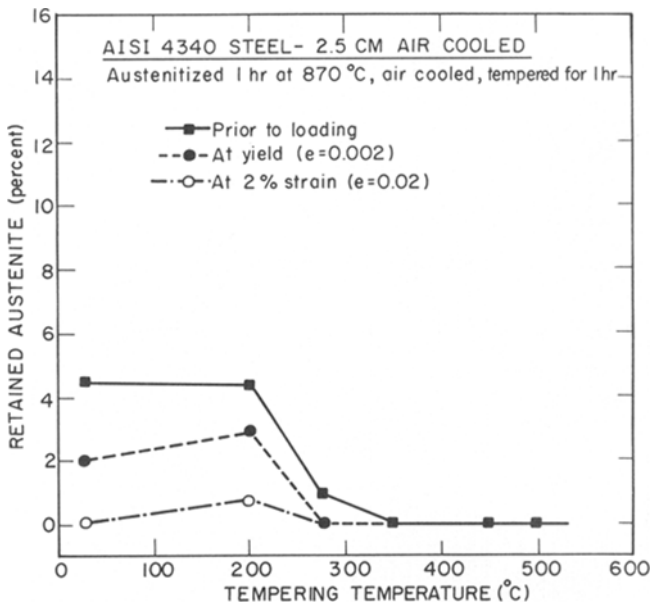

Fig. 18–Variation of percentage of retained austenite with tempering temperature for 4340 steel, air cooled (unstressed, 0.2 pct strain, 2.0 pct strain levels shown).

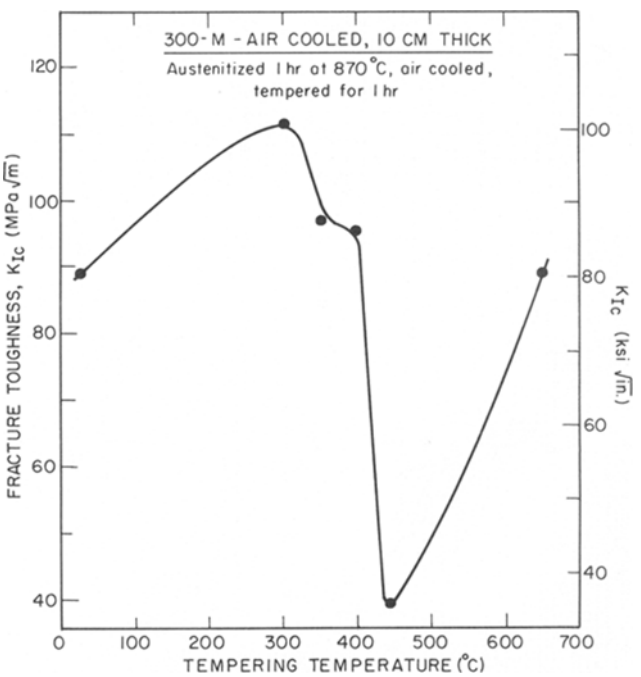

Fig. 19–Effect of tempering temperature on the plane strain fracture toughness for 300-M steel, air-cooled to represent 100 mm thick plate. (Note the 70 MPa$\sqrt{m}$ drop in toughness after tempering at 450°C.)

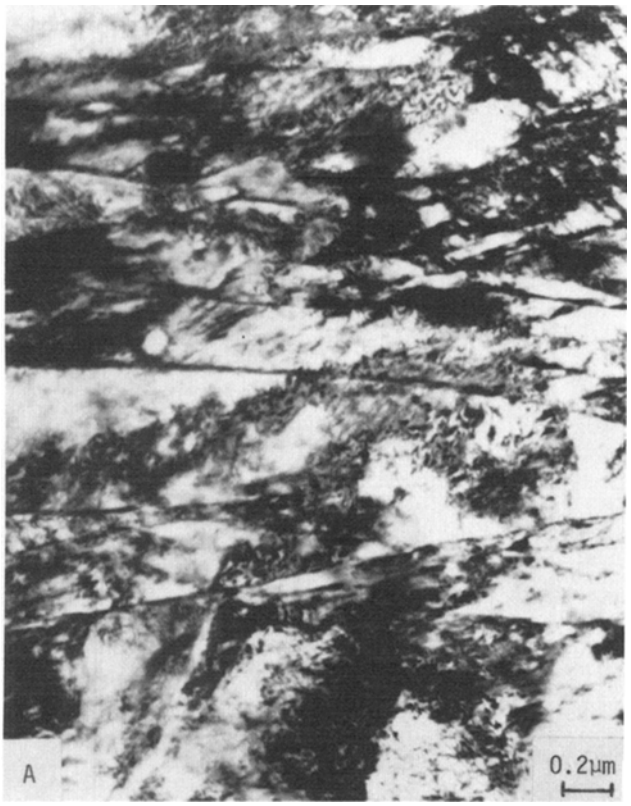

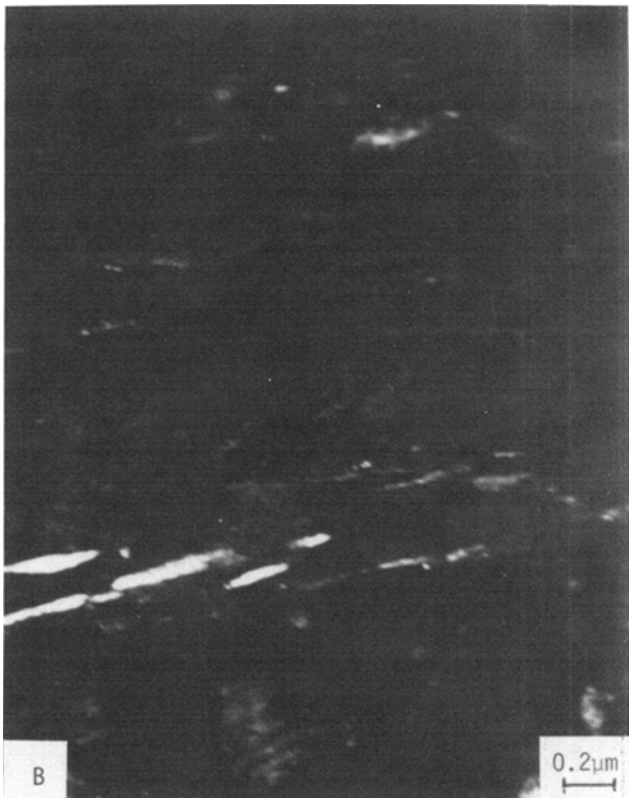

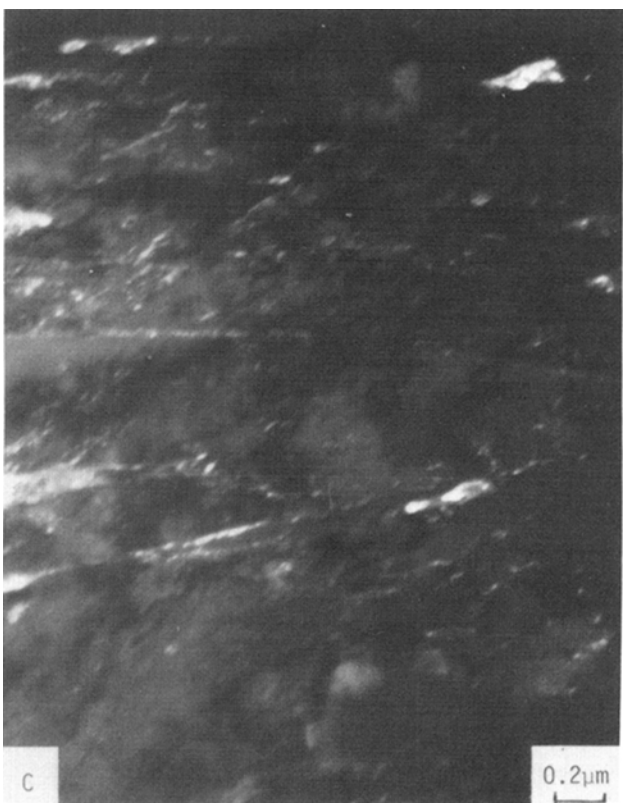

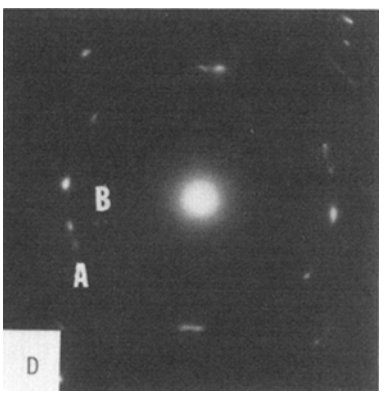

Fig. 20–Transmission electron microscopy of 300-M steel oil quenched and tempered at 400°C. (*a*) Bright field image revealing martensitic lath structure, (*b*) dark field image of $(200)_\gamma$ reverses contrast of austenite, (*c*) dark field image of $(\bar{1}0\bar{2})$ cementite reflection reverses contrast of discontinuous carbide film at lath boundary, (*d*) diffraction pattern of $[\bar{1}11]\gamma \| [0\bar{1}0]$ Fe_3C $\| [011]\alpha$ zones. *A* is $(200)\gamma$, *B* is $(\bar{1}0\bar{2})Fe_3C$.

steels could not be directly linked to the presence of austenite. However, refrigeration procedures[12] (and, incidentally, the commercially-used procedure of double tempering[13]) are only partially successful in removing austenite in low alloyed steels.* Furthermore, it has been clearly demonstrated in the present investigation and others[13-18] that intergranular fracture is not necessarily a characteristic of TME, particularly in these commercially important steels. In the present study, the largest embrittlement troughs in structures containing significant proportions of interlath austenite (300-M-AC and 300-M-ISO), were associated with an interlath cleavage mechanism of failure (Fig. 10(*b*)), whereas the smaller TME troughs, in structures with low austenite content (300-M-QT, 4340-QT and 4340-AC) were associated with transgranular cleavage (Fig. 16(*b*)) or mixed cleavage/microvoid coalescence (Fig. 5(*c*)) failures. The fact that no intergranular fracture was evident in embrittled samples in the present steels is not to discount the role of impurities on TME, since coarser grained structures may well give rise to some intergranular failure,[32] but merely serves to emphasize that impurity effects are not necessarily a dominant cause of TME.

*These added procedures reduce the austenite level approximately 2 to 4 pct.

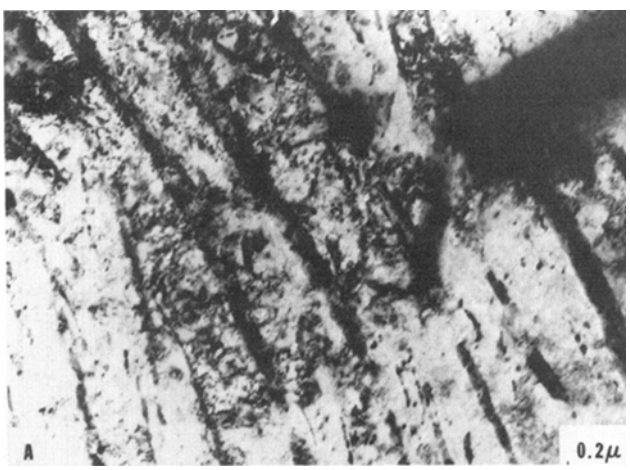

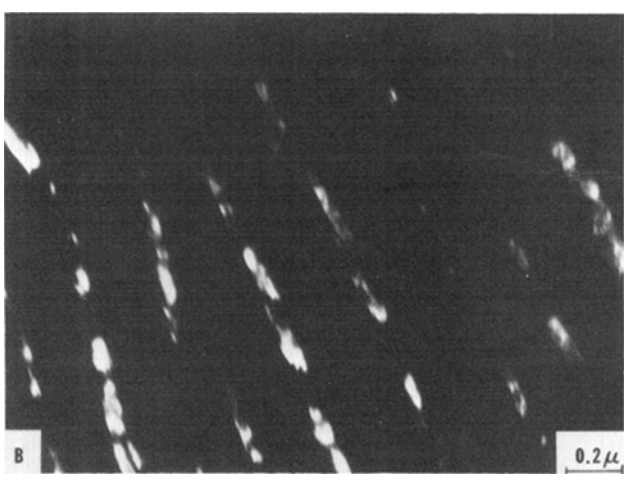

Fig. 21—Transmission electron microscopy of 300-M steel, air cooled and tempered at 470°C. (*a*) Bright field image of bainitic-martensite matrix containing retained austenite and cementite. (*b*) Dark field image of (200)γ reflection reversing contrast of austenite.

The other important feature of TME apparent from the present work was that, for all treatments studied, ϵ-carbide, identified as the hardening carbide at peak strength (and concurrent peak toughness), was replaced by cementite in the embrittlement range. Furthermore, transmission electron microscopy of embrittled structures (Fig. 20) revealed that the cementite had precipitated as discontinuous interlath films (Fig. 20(*c*)). Other authors have attributed the TME trough directly to interlath cementite precipitation. Thus, it is apparent that the onset of TME coincides both with *mechanical* destabilization of interlath films of austenite, and the replacement of ϵ-carbide by precipitation of interlath cementite. These two phenomena are clearly linked, since the carbide is precipitating in the same location as films of high carbon austenite. This is shown in Fig. 20 where dark field imaging of the lath structure in embrittled 300-M-QT (*i.e.*, tempered at 400°c), verifies the *simultaneous* presence of austenite and cementite on interlath boundaries. It is, therefore, considered that the sequence of TME is as follows. Austenite is retained as interlath films in as-cooled structures (*e.g.*, Figure 7) due to mechanical stabilization and thermal stabilization from slight partitioning of carbon during austenitizing in oil-quenched structures, or is retained in larger proportions due to significant carbon partitioning during air-cooling or isothermal holding in slow-cooled structures. This high carbon austenite on lath boundaries can then act as a primary source for the precipitation and growth of embrittling carbide films at austenite-martensite lath interfaces.* Once the carbide forms, the austenite becomes depleted in carbon, and accordingly becomes mechanically unstable. Table III lists the austenite lattice parameter (a_0) for 300-M-AC in different temper conditions. After tempering at 470°C, the austenite has experienced a decrease in a_0 consistent with carbon depletion. On deformation, the unstable austenite transforms to leave an embrittling film of untempered martensite on lath boundaries, in the same location as the embrittling cementite precipitates. It is not possible from the present study to discuss the relative contributions to the severity of TME from these two embrittling effects. However, we would postulate that in structures containing small volume fractions of retained austenite, such as 300-M-QT, 4340-QT, and 4340-AC, the embrittling effect of the interlath carbides is dominant. This is consistent with the fracture mode observed in embrittled samples of these structures which is primarily transgranular cleavage (Fig. 16), presumably initiated by the tensile cracking of grain boundary or interlath carbides. In structures containing large volume fractions of re-

*It has been recently shown[50] that cementite is precipitated directly from austenite in silicon-containing bainitic steels.

Table III. Austenite Lattice Parameter for 300-M-AC After Tempering

Tempering Treatment	Austenite, Pct	$a_0(311)\gamma$	$a_0(220)\gamma$
300°C	13.2	3.627Å	3.628Å
400°C	14.6	3.611Å	3.616Å
470°C	3.2	3.598Å	3.598Å

tained austenite, however, such as 300-M-AC and 300-M-ISO, the fracture mode in embrittled samples is interlath cleavage, which suggests that the embrittling effect of the layer of mechanically-transformed austenite (*i.e.*, untempered martensite) is dominant, consistent with the markedly increased severity of TME in these structures. Thus, a mechanism is proposed for tempered martensite embrittlement in ultra-high strength steels which relies on i) the precipitation and growth of embrittling cementite films on grain and interlath boundaries and ii) the concurrent thermal *and* mechanical destabilization of adjacent films of retained austenite (due to carbon depletion) as a consequence of this carbide precipitation, and iii) the embrittling effect of a consequent layer of mechanically-transformed austenite (interlath untempered martensite). The role of impuriteis is not ruled out as a mechanism for TME, since if the level of residual 'tramp' elements is sufficiently high, such elements may be already present in prior austenite grain boundaries due to segregation during austenitization[32,47] providing alternative 'easy paths' for failure. Separation would presumably initiate at weakened grain boundary carbide/matrix interfaces leading to intergranular fractures. However, it appears for the present structures that impurity effects are of secondary importance.

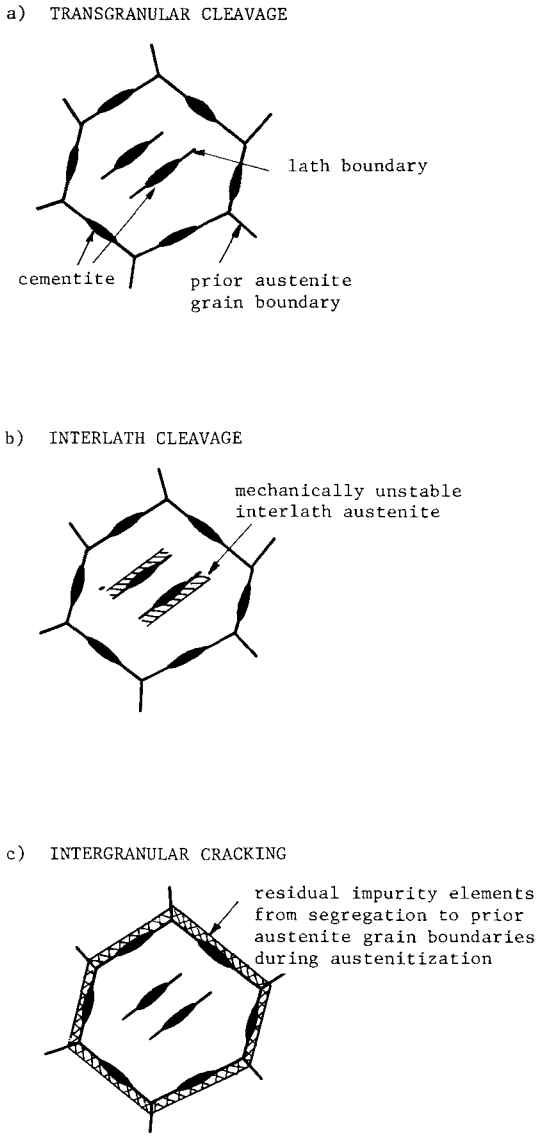

Fig. 22–Schematic diagrams of mechanisms of tempered martensite embrittlement showing resultant fracture modes due to: (*a*) cementite precipitation at lath and grain boundaries, (*b*) cementite precipitation and films of mechanically unstable retained austenite at lath boundaries, and (*c*) cementite precipitation and residual impurity elements at prior austenite grain boundaries. Cases (*a*), (*b*) or (*c*) tested at a temperature above the ductile to brittle transition temperature may exhibit ductile rupture or mixed mode.

Thomas[18] has recently proposed that the specific role of retained austenite on TME is the *thermal* destabilization of austenite at the embrittling tempering temperature resulting in thermal transformation to interlath carbide. This, however, is only partially correct since untransformed austenite is still present in *unstressed* embrittled structures (see Figs. 7, 12, 13, 17 and 18). This is clearly verified in Fig. 21, which shows the presence of retained austenite films in 300-M-AC tempered at 470°C (*i.e.*, at the 'bottom' of the TME trough in Fig. 8). The important fact is that, although a certain fraction of the austenite does transform thermally during tempering to form interlath carbide, the larger proportion remains thermally stable, but mechanically unstable, due to carbon depletion, and then transforms on subsequent loading.

In the context of the present work and previous research on a wide range of steels[1,33,47,48] we are now able to propose mechanisms for TME which account for the observed embrittlement fracture mechanisms; namely, transgranular cleavage, interlath cleavage, intergranular cracking, ductile rupture, or mixed mode. These are schematically illustrated in Fig. 22. It is clear that the essential feature of TME is embrittlement from cementite precipitation during tempering. In high strength steels, such as 4340, this occurs on grain and lath boundaries, aided by thermal decomposition of interlath films of austenite. In steels where the level of impurities and retained austenite is small, the dominant embrittlement mechanism is the tensile fracture of such carbides and the resulting fracture mode will be transgranular cleavage (*i.e.*, 4340-QT and 4340-AC). However, the consequence of interlath carbide precipitation is mechanical destabilization of the remaining interlath austenite, resulting in largely stress-assisted transformation to an interlath layer of untempered martensite. This provides an increasingly major contribution to embrittlement in microstructures containing larger volume fractions of austenite, resulting in an interlath cleavage fracture mode (*i.e.*, 300-M-ISO and 300-M-AC). In steels containing sufficient residual impurity content (*i.e.*, impurity-doped steels), or microstructures particularly susceptible to grain boundary embrittlement (*i.e.*, coarse-grained structures), such impurities, particularly P, will tend to segregate to prior austenite grain boundaries during austenitization.[32,47] In the embrittlement range, the combination of cementite precipitates *and* impurities in prior austenite grain boundaries will lead to the lowest cohesion at grain boundary carbide/matrix interfaces, resulting in intergranular fracture. Should

the temperature of testing be above the ductile/brittle transition temperature, mixed mode or fibrous fractures may result in the TME range. This is consistent with results that show, for certain steels, no TME at ambient temperature, yet marked embrittlement at −196°C,[47] and fractographic observations in the embrittlement range of mixed fibrous/intergranular fracture at ambient temperature and 100 pct intergranular fracture at −196°C.[48]

It is concluded that TME in a given steel cannot be generally attributed to a single mechanism, and in many cases all three mechanisms; namely those involving carbide precipitation, unstable austenite and impurity segregation, may act in concert, the resultant fracture mode merely indicating the weakest path. It is felt, however, that the present work, while confirming that the essential feature of TME is cementite precipitation, clearly documents the fact that the presence of interlath films of retained austenite can markedly affect the severity of this embrittlement.

CONCLUDING REMARKS

There has been much discussion recently on the beneficial role of retained austenite on the toughness of alloy steels, such as 4340[18,40-44]. It is apparent from the present paper, however, that before such claims can be made, it is essential to define the stability of the austenite *both thermally and mechanically*. With respect to TME, thermally unstable interlath austenite, with respect to tempering temperature, is clearly *not* beneficial, since the transformation product is interlath cementite, as similarly proposed by Thomas.[18] More importantly, mechanically unstable austenite, in the present steels,* is also clearly *not* beneficial, since the transformation product is untempered martensite which results in massive embrittlement troughs (Figs. 9, 10, and 19). Since retained austenite is similarly mechanically unstable in untempered structures, we would strongly question any claims[18,41,42] of an increase in toughness due to the presence of retained austenite in as-quenched steels, without evidence of its mechanical stability.

The question also arises whether *stable* retained austenite can be beneficial to toughness.* Several authors[18,41-44] have claimed this to be so, but comparisons were made at different strength levels,[18,44] between two different steels,[18] in untempered steels,[18,42] and in structures where other microstructural changes were not defined.[44] Furthermore, in no cases were the thermal and mechanical stabilities of the austenite unambiguously documented. In the present investigation, air-cooled or isothermally-transformed 300-M, after tempering at 300°C, is substantially tougher than the corresponding oil-quenched structure. Because these treatments lead to large volume fractions of retained austenite *and* lower strength, however, it can only be concluded that the presence of mechanically stable austenite does not appear to impair properties. The evidence to further suggest that the presence of retained austenite leads directly to toughness increases (without strength loss) is inconclusive.

*Large *increases* in toughness in higher alloyed steels (*i.e.*, 10 pct Cr-9 pct Ni-5 pct Mo) of lower carbon content (0.2 pct) have been ascribed to the strain-induced transformation of mechanically unstable austenite, (the basis of "TRIP" Steels[45]). The reasons for this marked difference in behavior compared to the present 4340-type steels are most likely related to i) the transformation product in the higher carbon 4340 steel will be a more brittle (higher carbon) martensite, and ii) the embrittling effect of mechanically unstable austenite in 4340 steels occurs after a principally stress-assisted transformation (*i.e.*, a large proportion of the austenite has transformed before yield); and iii) the transformation in the 4340-type steels occurs in hardened, low-ductility matrix.

*Related work on the influence of mechanically stable retained austenite on other properties suggest that the presence of a continuous interlath network of this phase in bainitic/martensitic structures in 300-M can significantly improve resistance to stress-corrosion cracking when compared to quenched and tempered structures, containing no austenite, at equivalent strength,[39] and marginally improve resistance to very low growth rate, near-threshold, fatigue crack propagation when compared at equivalent cyclic strength.[46]

CONCLUSIONS

Based on a study of the phenomenon of tempered martensite embrittlement (TME) in commercial ultra-high strength 4340 and Si-modified 4340 (300-M) alloy steels subject to quench and tempering, isothermal transformation and air-cooling heat-treatments, the following specific conclusions can be made:

1) TME is manifest as a decrease in toughness, measured both in K_{Ic} and Charpy V-notch impact energy data, after tempering at around 275°C in 4340 and around 400 to 470°C in 300-M.

2) The embrittlement is concurrent with the replacement of ϵ-carbide by interlath cementite during tempering, *and* the mechanical instability of interlath films of austenite (as a consequence of this carbide precipitation) during subsequent loading.

3) The displacement of TME to higher tempering temperatures in 300-M, due to the increased silicon content, results from the effect of this element enhancing the stability of ϵ-carbide, retarding the formation and growth of cementite and consequently increasing the thermal and mechanical stability of retained austenite at higher tempering temperatures.

4) The severity of TME is directly related to the volume fraction of interlath, retained austenite present. Isothermally-transformed and air-cooled 300-M, containing greater than 12 pct retained austenite, are therefore significantly more susceptible to TME than structures containing low volume fractions of austenite.

5) The mechanisms of fracture in embrittled structures was found to be interlath cleavage in microstructures containing large percentages of interlath austenite (*i.e.*, which show severe embrittlement), and transgranular cleavage or mixed cleavage/microvoid coalescence in microstructures containing low percentages of austenite. No evidence of intergranular cracking was detected.

6) A new mechanism of tempered martensite embrittlement is proposed involving i) precipitation of interlath cementite aided by partial thermal decomposition of interlath films of retained austenite, and ii) subsequent deformation-induced transformation on loading of remaining interlath austenite, which has become mechanically unstable due to carbon depletion as a consequence of this carbide precipitation.

In addition, the following general conclusions on the nature of TME can be made:

1) The essential feature of TME is the precipitation during tempering of brittle cementite on grain and lath boundaries. Lath boundaries may also contain layers of mechanically-unstable austenite, as a consequence of this carbide precipitation, whereas grain boundaries may also contain residual impurity elements, as a consequence of segregation during austenitization.

2) In steels containing large volume fractions of austenite, the combination of cementite precipitates and mechanically unstable austenite on *lath boundaries* leads to fracture by interlath cleavage in the embrittlement range, and to the most severe form of TME.

3) In steels which contain significant impurity levels or are particularly susceptible to impurity-induced embrittlement, the combination of cementite precipitates and residual impurity elements on prior austenite *grain boundaries* leads to fracture by intergranular cracking in the embrittlement range.

4) In steels containing small levels of austenite and impurities, the tensile cracking of brittle cementite precipitates on grain and lath boundaries leads to fracture by transgranular cleavage in the embrittlement range.

5) In steels tested at temperatures greater than the ductile/brittle transition temperature, fracture in the embrittlement range may additionally involve ductile rupture.

ACKNOWLEDGEMENTS

The research was conducted under the auspices of the U.S. Energy Research and Development Administration through the Materials and Molecular Research Division of the Lawrence Berkeley Laboratory. The authors wish to thank Professors E. R. Parker and V. F. Zackay for their constant help, support, and encouragement, and Mr. J. R. Dillion and Dr. M. S. Bhat for experimental assistance. Many long, and often heated, discussions with Professors Cohen, McMahon, Owen, Thomas, Parker, Zackay, and Drs. Banerji, Bhat, Briant, Knott, and Rao on the nature of this topic are also warmly acknowleged.

REFERENCES

1. J. R. Low, Jr.: in *Fract. Eng. Mater.*, ASM, 1964, p. 127.
2. C. J. McMahon, Jr.: ASTM STP 407, p. 127, American Society for Testing and Materials, 1968.
3. E. B. Kula and A. A. Anctil: *J. Mater.*, 1964, vol. 4, p. 817.
4. B. J. Schulz and C. J. McMahon, Jr.: ASTM STP 499, p. 104, American Society for Testing and Materials, 1972.
5. M. A. Grossmann: *Trans. AIME*, 1946, vol. 167, p. 39.
6. H. Schrader, H. J. Wiester, and H. Siepmann: *Arch. Eisenhuettenw.*, 1950, vol. 21, p. 21.
7. R. L. Rickett and J. M. Hodge: *Proc. ASTM*, 1951, vol. 51, p. 931.
8. L. J. Klingler, W. J. Barnett, R. P. Frohmberg, and A. R. Troiano: *Trans. ASM*, 1954, vol. 46, p. 1557.
9. J. J. Irani, M. J. May, and D. Elliott: ASTM STP 407, p. 168, American Society for Testing and Materials, 1968.
10. E. J. Ripling: *Trans. ASM*, 1950, vol. 42, p. 439.
11. G. V. Luerssen and O. V. Greene: *Ibid*, 1935, vol. 23, p. 861.
12. L. S. Castleman, B. L. Averbach, and M. Cohen: *Ibid*, 1952, vol. 44, p. 240.
13. R. M. Horn: Ph.D. Thesis, University of California at Berkeley, 1976 (Lawrence Berkeley Laboratory Report No. LBL-5787, December 1976).
14. V. H. Lindborg and B. L. Averbach: *Acta Met.*, 1966, vol. 14, p. 1583.
15. E. F. Walker and M. J. May: ISI Publ. 120, p. 135, 1970.
16. W. Backfisch and K. H. Schwalbe: Proc. Fourth International Conf. on Fracture, Waterloo, vol. 2, p. 73, 1977.
17. J. E. King, R. F. Smith, and J. F. Knott: *Ibid*, vol. 2, p. 279.
18. G. Thomas: *Met. Trans. A*, 1978, vol. 9A, p. 439.
19. A. Nakashima and J. F. Libsch: *Trans. ASM*, 1961, vol. 53, p. 753.
20. B. S. Lement, B. L. Averbach, and M. Cohen: *Ibid*, 1954, vol. 46, p. 851.
21. A. J. Baker, F. J. Lauta, and R. P. Wei: ASTM STP 370; p. 3, American Society for Testing and Materials, 1963.
22. R. D. Goolsby: Ph.D. Thesis, University of California in Berkeley, 1971 (Lawrence Berkeley Laboratory Report No. LBL-405, November 1971).
23. A. G. Allten and P. Payson: *Trans. ASM*, 1953, vol. 45, p. 498.
24. C. H. Shih, B. L. Averbach, and M. Cohen: *Ibid*, 1956, vol. 48, p. 86.
25. C. J. Altstetter, M. Cohen, and B. L. Averbach: *Ibid*, 1962, vol. 55, p. 287.
26. M. S. Bhat: Ph.D. Thesis, University of California at Berkeley, 1977 (Lawrence Berkeley Laboratory Report No. LBL-6046, February 1977)
27. W. S. Owen: *J. Iron Steel Inst.*, 1957, vol. 177, p. 445.
28. B. R. Banerjee: ASTM STP 370, p. 94, American Society for Testing and Materials, 1963.
29. B. R. Banerjee: *J. Iron Steel Inst.*, 1965, vol. 203, p. 166.
30. J. M. Capus and G. Mayer: *Metallurgia*, 1960, vol. 62, p. 133.
31. J. R. Rellick and C. J. McMahon, Jr.: *Met. Trans.*, 1974, vol. 5, p. 2439.
32. S. K. Banerji, C. J. McMahon, Jr., and H. C. Feng: *Met. Trans. A*, 1978, vol. 9A, p. 237.
33. R. M. Horn and R. O. Ritchie: *Proc. 106th Annual AIME Meeting*, Atlanta, March 1977.
34. F. J. Witt: *Practical Application of Fracture Mechanics to Pressure-Vessel Technology*, p. 163, The Institute of Mechanical Engineers, London, 1971.
35. J. D. Landes and J. A. Begley: Westinghouse Scientific Paper 76-1E7-JINTF-P3, May 1976, Westinghouse Research Laboratories, Pittsburgh, Pa. 15235.
36. R. O. Ritchie, G. G. Garrett, and J. F. Knott: *Int. J. of Fract. Mech.*, 1971, vol. 7, p. 462.
37. B. D. Cullity: in *Elements of X-Ray Diffraction*, p. 391, Addison-Wesley Publ. Co. Inc., Reading, Mass., 1959.
38. D. Bhandarkar, V. F. Zackay, and E. R. Parker: *Met. Trans.*, 1972, vol. 3, p. 2619.
39. R. O. Ritchie, M. H. Castro-Cedeño, V. F. Zackay, and E. R. Parker: *Met. Trans. A*, 1978, vol. 9A, p. 35.
40. C. W. Marschall, R. F. Hehemann, and A. R. Troiano: *Trans. ASM*, 1962, vol. 55, p. 135.
41. J. McMahon and G. Thomas: *Proc. Third Int'l Conf. on the Strength of Metals and Alloys*, vol. 1, p. 180, Cambridge, Institute of Metals, London, August 1973.
42. G. Y. Lai, W. E. Wood, R. A. Clark, V. F. Zackay, and E. R. Parker: *Met. Trans.*, 1974, vol. 5, p. 1663.
43. B. V. N. Rao, J. Y. Koo, and G. Thomas: *Proc. Electron Microscopy Society of America*, p. 30, Claitors Publication Division, Baton Rouge, 1975.
44. K. J. Kim and L. H. Schwartz: *Mater. Sci. Eng.*, in press.
45. W. W. Gerberich, P. L. Hemmings, V. F. Zackay, and E. R. Parker: in *Fracture 1969*, p. 288, Proc. Second Int'l. Conf. on Fracture, Brighton, 1969, Chapman and Hall, Ltd., London.
46. R. O. Ritchie: *J. Eng. Mater. Technol.*, Trans. ASME Series H, 1977, vol. 99, p. 195.
47. C. L. Briant and S. K. Banerji: Unpublished research, General Electric Co., Schenectady, New York, 1977.
48. R. O. Ritchie: Ph.D. Thesis, University of Cambridge, 1973.
49. G. Y. Lai, W. E. Wood, E. R. Parker, and V. F. Zackay: Lawrence Berkeley Laboratory Report No. LBL-2236, University of California, April, 1975.
50. Der-Hung Huang and G. Thomas: *Met. Trans. A*, 1977, vol. 8A, p. 1661.